Fabrication of a test artifact for WAAM

Lourenço Dias
lourenco.dias@tecnico.ulisboa.pt

Instituto Superior Técnico, Universiade de Lisboa, Lisboa, Portugal

October 2020

Abstract

With the current increasing interest in metal additive manufacturing, caused by its capacity to reduce both material waste and lead times of each part, comes a subsequent growing need of test artifacts that allow to further increase the extent of these advantages. Be that as it may, there isn't a test artifact dedicated to the exclusive analyses of WAAM produced parts. As such, in this work, a test artifact was developed, comprised of: a 60^o inclined wall; a set of thin pins that progressively reduced in diameter until the setup failed to replicate the CAD model's dimensions; a set of thin resolution holes, whose diameter also progressively reduced until dimensional failure was achieved; two sets of straight walls oriented both along the X and Y axes; a cross shaped intersection; a staircase vertical increment. Upon deposition parameters optimization, the results revealed the thinnest features possible to print on the selected setup, as well as the range of inclination at which was possible to produce inclined walls. Moreover, it was possible to assess how the setup dealt with geometries with intersections and cross-overs, as well as geometries with increasing internal heat accumulation. More importantly, the test artifact created allowed to pinpoint several hardware and software limitations in addition to allowing to evaluate the performance of the robotic arm's along the X, Y and Z axes, and look for any existing miscalibrations or deviations.
Keywords: Wire Arc Additive Manufacturing (WAAM), test artifact, benchmark geometries, setup evaluation, hardware/software limitations, dimensional accuracy, axes deviations.

1. Introduction

The aid of test artifacts is indubitably an important tool for all processes of additive manufacturing (AM). A test artifact is comprised of a group of benchmark geometries designed to evaluate a specific feature or aspect of the parts produced by a certain setup. These geometries can aim at: revealing the geometric limits a setup can achieve, such as the thinnest features that are possible to prin;, recreate challenging geometries such as overhangs or intersections and cross-overs; provide the user with the accuracy of each building axes, ie, the X, Y and Z axes, identifying any miscalibrations or deviations existing; Pinpoint setup related limitations, either regarding software or hardware components. The use of test artifacts then gives the user the possibility to test certain geometries and equipment, without the need to resort to trial and error on potentially large parts, thus promoting both time and material savings.

Depending on the AM processes in question, the benchmark geometries can become more or less demanding, depending on the accuracy of the process. However such has not been the case for wire arc additive manufacturing (WAAM), an electric arc-based metal additive manufacturing process, that combines the use of welding equipment such as the feeding system, power source and welding torch, with the aid of a robotic arm to ensure the transportation of the welding torch through the substrate where the deposition will take place. As WAAM is a process often more adequate for medium to large scale parts , it can struggle when performing smaller features. However, as of yet, there is not a test artifact designed for WAAM produced parts, accounting for such geometrical limitations, and instead, the users are forced to use generic metal AM test artifacts, with geometries that are too demanding for WAAM to accomplish and provide the user with the desired information.

2. Background

2.1. Test Artifacts

As mentioned previously, a test artifact is a set of benchmark geometries destined to evaluate different aspects of the produced part. According to [1] three distinct properties can be evaluated: mechanical, geometric and surface properties. For the objectives of this work, only the geometric properties and their respective test artifacts, the geometric benchmark test artifacts (GBTA's), are of interest

to evaluate. As such all references made of test artifacts throughout the document are specifically in regards to GBTAs.

As reported by [2], when creating a new test artifact, certain characteristics must be included, such as: have holes and protrusions; be quick to produce and have low material requirements; be easy to measure and control the geometry of the part; must not require treatments after its fabrication; have features of real parts, such as thin walls and flat surfaces.

2.2. International Standard

In order to maintain homogeneity and consistency within all the measurements performed on the test artifacts, an international standard was developed, the ISO-ASTM 52902 Standard [3], presenting several guidelines that should be taken into considerations when gathering the results. From within the presented guidelines and requirements, the following are highlighted:

- All deposition strategies and parameters, for every geometry, must be presented, in order to ensure that any user can replicate them;
- In order to prevent deformations to the artifact's geometries, there mustn't be a need for suport structures nor surface treatments on the part. For the same reason, all measurements should be performed after letting the parts cool down to room temperature and without removing the geometries from the substrate;
- A minimum of three distanced measurements should be performed, preferably as represented on figure 1.

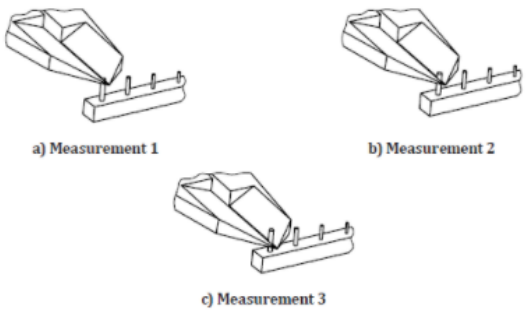

Figure 1: Illustration of the minimum amount of measurements per dimension. Example of thin resolution pins [3].

3. Implementation

3.1. Setup Description

Since the use of a test artifact will provide information regarding a setup, on must first identify said setup. For the purpose of this work, all components that are responsible for the part's deposition, as well as the planning and generation of the deposition paths, are considered part of the setup, meaning that there are both hardware and software elements.

The setup selected was comprised of a Fronius CMT VR 700 arc wire feeder, a CMT weld torch, a robotic arm responsible for the movement of the welding torch, more precisely a 6-Axis KUKA KR 150 L110-2 F 2000, and for the deposition path generation, WAAMSoft, a software developed by Cranfield University. Regarding the consumable materials, AWS A5.18 ER70S-6 ø= 1.2 mm consumable welding wire was used, as well as DIN 2391 ST 52 steel substrate plates and 18% carbon dioxide + 82% argon protective atmosphere.

Additionally, some considerations are important to retain, in order to ease the readers interpretation:

- As the deposition path generating software environment is considered to have 2.5 dimensions [4], when mentioning a vertical direction whilst in this environment, it's meant as along the Y axis direction. However, when analysing the deposited parts, as it's a 3D environment, the vertical directions coincides with height of the parts, ie, along the Z axis. The respective environments coordinate axis are presented in figure;
- Due to a software derived limitation, all depostions took place with the welding torch perpendicular to the substrate, ie, whilst maintaining a 90^o angle with the substrate.

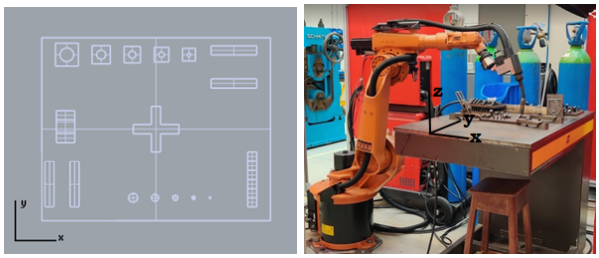

(a) Coordinate axes within the software. (b) Coordinate axes outside the software.

Figure 2: Different coordinate axes, for the different setup environments.

3.2. Geometry Selection

As previously mentioned, the evaluation of the setup is performed resorting to the use of benchmark geometries. As such, the following geometries were selected to incorporate the test artifact:

Overhanging structures: one of WAAM's most challenging geometries, not only as the resort of supporting structures should be avoided, but also

as a consequence of the forces inherent to the deposition process, as represented in figure 3, in which G is the force produced by gravity, Fa is the arc force,Fd is the force of the droplets impact and σ is the force generated by the surface tension of the molten pool.

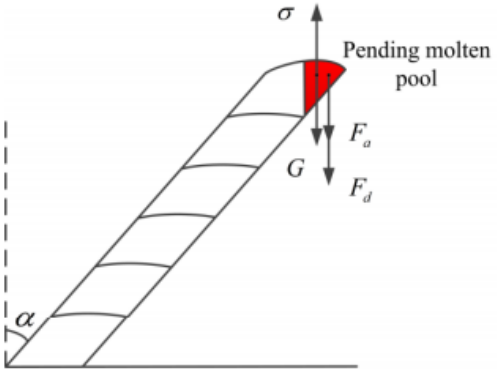

Figure 3: Representation of a force model during the fabrication of a inclined wall [5].

As it's possible to infer by the image above, the majority of the forces during the deposition and solidification of the molten material, are exerted downwards, pulling the molten material towards the substrate, and if the material doesn't present enough surface tension, might result in the structure's collapse. The most extreme cases of such are the fully overhanging structures (figure 4) that, as [6] states, are unbuildable when recurring to a conventional WAAM setup, as is the case. Therefore, the geometry selected to begin the study of overhanging structures was an inclined wall, making up 60^o with the substrate.

Figure 4: Structure with a fully overhanging feature decomposed into buildable and unbuildable subvolumes [6].

Thin pins: a fundamental geometry to discover the finest detail that's possible to manufacture. For this purpose, a series of pins with progressively smaller diameter were designed and are presented in figure 5, ranging from 10mm to 4mm, and all of which with a height of 30mm . A pin was considered satisfactorily built if it met its geometrical requirements: Having a cylindrical shape, with a clearly round section, and accurate dimensions, when compared to its digital model.

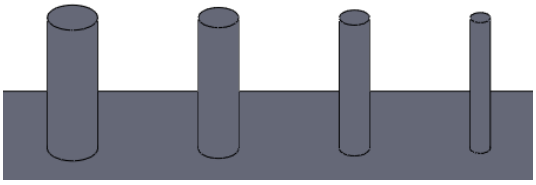

Figure 5: Thin pins with 10mm, 8mm, 6mm and 4mm respectively.

Thin resolution holes: similarly to the thin pins, this geometry allows to determine the finest hole possible to print. Similarly to the thin pins, the resolution holes also progressively reduced in diameter, starting with a 15 mm diameter hole and advancing to 10 mm, 8 mm, 6 mm and 4 mm diameter holes (figure 6). It's important to note however, that despite the diameter of the hole changing from part to part, the height and thickness of the parts were kept constant. The height was maintained at 20 mm and the thickness at 5 mm, in order to ensure that there were similar conditions between parts, regarding heat transfer.

Ultimately, this meant the the manufacture of this part also allowed to analyse how parts built dealt with the decrease of the hole and, consequently, decrease of the available surface are to promote heat exchange. Once the heat exchange becomes insufficient, the molten material will take longer to solidify which might cause it to drip, and thus failing to replicate the intended dimensions.

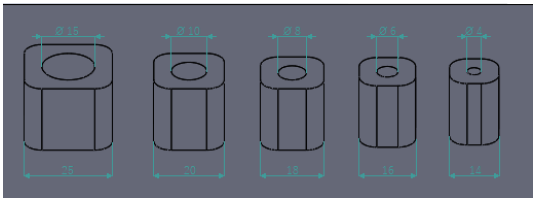

Figure 6: CAD model of the thin vertical resolution holes and respective dimensions in mm.

Moreover, the corners' fillet radius was also kept constant, meaning that as the distance between corners decreases, the distinction between the corners and the straight sections will become harder to perform.

Finally it's important to highlight that the primary objective of this test isn't to create the smallest hole possible with the equipment in question, but rather to accurately replicate the measurements of the CAD model, both of the diameter of the hole and the surrounding structure, whilst still maintaining the desired geometrical shape.

Straight walls: this simple geometry is divided in the test artifact into two sets of two identical

and parallel straight walls, with a length of 50 mm, width of 10 mm and a height of 20 mm (figure 7). One of the sets is aligned with the X axis, while the other is aligned with e Y axis, thus providing information regarding the deposition precision of both axes.

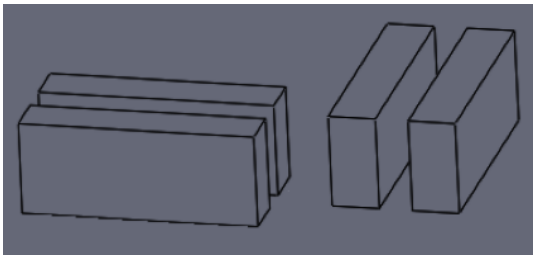

Figure 7: CAD model of the straight walls.

Additionally, as the walls within each set are parallel to each other, it's also possible to evaluate the setup's capacities to maintain parallelism. Additionally, different depositions strategies could be employed for each of the walls in both sets, thus providing a side-to-side comparison of both strategies

Cross shaped intersection: This geometry allows to not only corroborate any previously obtained information regarding the X and Y axes deviations, but also to test how the setup performs intersections in which there is a complete overlap of two deposition segments. A deposition with an excess of deposited material will result in the formation of a hump, while a lack of material on the junction area will promote a contraction and shrinkage of the part.

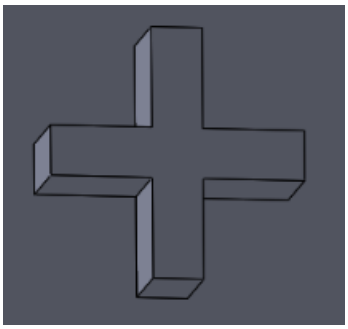

Figure 8: CAD model of the cross shaped intersection.

For this purpose, two rectangular segments, similar to ones mentioned above (length of 50 mm, width of 10 mm and a height of 20 mm), were placed perpendicularly to each other, hence creating the shape of a cross (figure 8).

Staircase vertical increment: the final geometry targets to evaluate how the increase of heat accumulation affects a constant vertical increment. In order to achieve this, a staircase shaped structure was devised, were the first step, ie, the lowermost increment of the part, has a height of 10 mm while all other five increments measure 5 mm, thus comprising a total part height of 35 mm. Additionally, all steps both have a constant width and length of 10 mm, making up a total part length of 60 mm (figure 9).

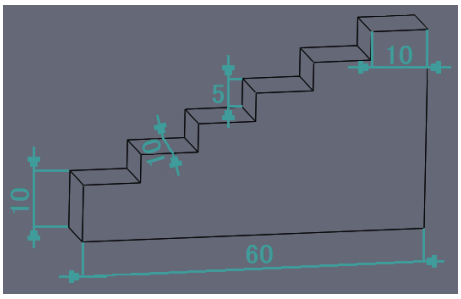

Figure 9: CAD model of the staircase vertical increment and key dimensions in mm.

4. Results

The following section will present the parameters that were found to be most effective for each geometry, as well as the respective final dimensions. Additionally all of the setup induced limitations will be exhibited as well.

4.1. Inclined Wall

As expected, the 60^o inclined wall was one of the most challenging geometries to perform. It was found that, in order to achieve a successful deposition, two main properties had to be simultaneously adjusted: the heat input and the $\frac{WFS}{WTS}$ ratio.

The process's heat input [J/mm] refers to the amount of energy [J] that is provided by unit of length [mm], and can be calculated using equation 1, where V and I are the voltage and the current of the process respectively and η is the welding process efficiency. This last variable is dependent on the welding process selected and the equipment used. For all calculations on this work, a value of 0.85 was selected, in accordance with the source material found [7, 8].

$$HI = \eta \frac{V \cdot I}{WTS} \tag{1}$$

The $\frac{WFS}{WTS}$ ratio is attained by dividing the wire feed speed (WFS), the velocity at which the torch provides the wire feedstock, by the wire travel speed (WTS), the velocity at which the torch moves along the substrate. This ratio can then provide the user with a reference of material accumulation, that is, the amount of molten material deposited per unit of length of the part.

As mentioned previously, the adjustment of both these parameters was necessary to prevent deposition failure. If the $\frac{WFS}{WTS}$ ratio is to high, there will be an excess of material, and the part will consequently collapse. If the same ratio is too low, then there wont be enough deposited material to generate the intended layer. This in turn will cause the part to have a deformation, as there's a lack of material. All the while, as the robotic arm can't detect this deformation, it will carry on with the deposition and might result in the deposition of material outside the part and onto the substrate.

On the other hand, several parts can have the exact same $\frac{WFS}{WTS}$ ratio and still produce very different outcomes, as seen in figure 4.2. The difference lies in the heat input value. A high heat input can result in the part's failure to reduce the molten material's temperature, and eventually lead to its collapse. However, the study of this geometry revealed that a slight increase of this property can be beneficial for the success of the geometry. A minor increase in the heat input can cause the layer directly bellow the one deposited to reheat, to such a point were, whilst being subjected to a downwards force, caused by the layer of material above it, it becomes flattened. This effect allows to offset a possible deformation to the parts caused by a lack of deposited material, as discussed formerly.

(a) Inclined wall with $WFS = 3m/min$ and $WTS = 3m/min$.

(b) Inclined wall with $WFS = 3.5m/min$ and $WTS = 3.5m/min$.

(c) Inclined wall with $WFS = 5m/min$ and $WTS = 5m/min$.

Figure 10: Examples of different outcomes for the same $\frac{WFS}{WTS}$ ratio, in the deposition of inclined walls.

Upon parameter optimization, a satisfactory final geometry was achieved (4.2 (b)), using the following parameters: layer height of 2.75mm, $WFS = 3.5m/min$, $WTS = 3.5m/min$, and thus, $\frac{WFS}{WTS} = 1$.

Despite achieving the final goal of building a 60^o inclined wall, the process was undermined by the inability of the software used to alter the deposition strategy, forcing the user instead to only rely on a oscillating deposition strategy. Resorting to a different strategy, such as a unidirectional deposition would have reduced the part's heat accumulation [9], possibly allowing better results and perhaps a further decrease of the overhang angle.

4.2. Thin Pins

As the main goal for this geometry is to perform the thinnest feature possible, it's helpful to select the lowest value available for the WFS, thus depositing as few material as possible. However, it was found that when using WFS values that were inferior to 3m/min, the setup failed to ignite and stabilize the electric arc, due to the inherent low values of both the voltage and electric current. Consequently, the minimum WFS value was then set at 3m/min.

The measurements obtained for each pin along with their respective deposition parameters are presented hereinafter:

Table 1: Thin pins final parameters.

	WFS [m/min]	WTS [m/min]	Layer Height [mm]	Parcel Distance [mm]
10 mm pin	3	6	1.7	2.5
8 mm pin	3	6	1.5	3
6 mm pin	3	10	1.2	3
4 mm pin	3	30	0.9	2

Table 2: Thin pin's final measurements and respective deviations from the CAD.

	10 mm pin	8 mm pin	6 mm pin	4 mm pin
Part's Height [mm]	30.6	29.5	30	30.6
Height Deviation [mm]	0.6	-0.5	0	0.6
X-Axis Diameter [mm]	10.1	8.1	6.4	5.2
X-Axis Deviation [mm]	0.1	0.1	0.4	1.2
Y-Axis Diameter [mm]	9.7	8.1	6.2	5.2
Y-Axis Deviation [mm]	-0.3	0.1	0.2	1.2

As it's possible to infer, the setup failed to accurately replicate the pin with a diameter of 4 mm, generating instead a diameter of 5.2 mm, 1.2 mm off the target dimension. This building limit was imposed by the software used, as it requires both a start and end point in order to generate a deposition path. This in turn means that it was not possible to perform a single-point deposition, ergo increasing the minimum diameter that would be possible to attain.

Furthermore, it's worth mentioning that the overall tendency was for the measurements deviation to increase with the decrease of the pin's diameter. This became more evident on the case of the last produced pin. Although part of this dimensional

difference is cause by the previously mentioned software limitation, it's also possible to assume that some additional vibrations and consequent uncertainty, were caused by the high travel speed selected in order to decrease the diameter of the pin.

4.3. Thin Resolution Holes

Unlike the previously analysed cases, in order to perform a successful deposition of this geometry, there are three different types of dimensions that need to be taken into consideration:

- **Internal dimensions:** the measurements of the hole in the X and Y axes;
- **External dimensions:** he measurements of the external structure that contains the hole, also both the X and Y axes;
- **Part's height**.

As the objective when building a benchmark geometry is to accurately replicate all of the CAD's dimensions, all three types of dimensions must be adequately replicated in order to the deposition be considered successful, thus advancing to the following hole with a smaller diameter.

Once again, this geometry benefits from the use of a minimal WFS value, in order to prevent the deposition of an excessive amount of material, resulting in an incorrect hole diameter. As such, a WFS of 3 m/min was selected once more, while varying the layer height, the wire travel speed and the distance between deposition paths.

Once more, it was concluded that the software handicapped the deposition of this geometry as well. Firstly, it was not possible to generate a deposition path for a part with a hole within it, such as the one in selected geometry, as the software couldn't recognize a segment that encompassed the entirety of the geometry. This meant that the part had to be separated into two separate segments, thus creating a new problem: instead of one uniform part, this strategy generated two parts that had to be connected in a seamless way.

Moreover, upon the analyses of the deposited parts, it was possible to detect a duality within the resulting part dimensions. While it was possible to achieve the desired diameter, and thus replicating the part's internal dimensions, the same was not possible regarding the external dimensions, as these were shorter than expected. Contrarily, when trying to correct the external dimensions by reducing the WTS, thus increasing the amount of material deposited, as well as altering the deposition parcel distance, the internal dimensions then became smaller that intended. It then become clear that it was not possible to replicate them both successfully. This effect was suspected to be caused by a miscalculation within the software, therefore generating a deposition path that was shorter that one actually needed.

Tables 3.3 and 3.4 present the final part's deposition parameters and the final measurements and deviation's from the CAD model, respectively.

Table 3: Thin vertical resolution holes final parameters.

	WFS [m/min]	WTS [m/min]	CZ [m/min]	LH [mm]	Parcel Distance [mm]
15 mm hole	3	13	7	1.5	3.5
10 mm hole	3	16	9	1.25	3.5
8 mm hole	3	28	16	1.25	2.5

Table 4: Thin vertical resolution hole's final measurements and respective deviations from the CAD.

	15 mm hole	10 mm hole	8 mm hole
Part's Height [mm]	20.5	19.9	19.7
Height Deviation [mm]	0.5	-0.1	-0.3
X-Axis Hole Diameter [mm]	14.9	9.9	7.5
X-Axis Hole Diameter Deviation [mm]	-0.1	-0.1	-0.5
Y-Axis Hole Diameter [mm]	14.2	9.8	7.8
Y-Axis Hole Diameter Deviation [mm]	-0.8	-0.2	-0.3
External X-Axis Length [mm]	24.6	19.3	16.1
External X-Axis Length Deviation [mm]	-0.4	-0.7	-1.9
External Y-Axis Length [mm]	24.5	19.3	15.4
External Y-Axis Length Deviation [mm]	-0.5	-0.7	-2.6

(a) Final 15 mm thin resolution hole.

(b) Final 10 mm thin resolution hole.

(c) Final 8 mm thin resolution hole.

Figure 11: Final results for all the attempted thin resolution holes.

After analysing the results, it's possible to verify that both the 15 mm and the 10 mm hole parts were successfully built, while during the 8 mm, the discussed duality prevented the part's success, ergo stopping the test of this geometry. However, it's important to reinstate that the failure came from the external dimensions and not from the internal,

as it was initially expected. It's then not possible to state that the minimum buildable internal diameter was found, despite the fact that a setup limit had been reached.

Proceeding with the parts geometrical analyses, it's possible to see that there were no significant differences in terms of deposited material along the areas with changes of direction. Although an occasional hump appeared, it was not consistent within all changes of direction. Instead it only arose at the end of each deposited layer, hence suggesting a different problem, that will in turn be discussed further on this work. It's then possible to infer that the present setup is adequate to perform changes of direction, as it is capable to compensate the differences in linear travel speed when doing so.

Furthermore, despite presenting an increasing difficulty to clearly distinguish the part's straight walls from its rounded corners, the setup ended up separating the two features satisfactorily. It's however expected that for parts with a smaller diameter, the setup will not be able to distinguish them, resulting in the merge of the four corners, and cylindrical final geometry.

4.4. Straight Walls

As previously mentioned on section 3.2, with this geometry the user could simultaneously test two distinct deposition strategies. As it was already established that the software used only supported the use of oscillating depositions, two variants of this strategies were tested: a deposition path using a horizontal deposition guide line, and another with a vertical deposition guide line, as see in figure 12.

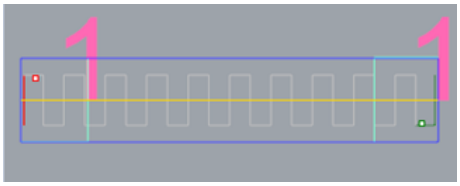

(a) Deposition strategy with a horizontal deposition guide line.

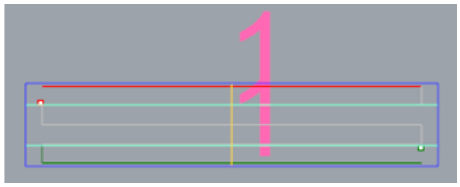

(b) Deposition strategy with a horizontal deposition guide line.

Figure 12: Different deposition strategies used for the straight walls.

While manufacturing this geometry, an unintended effect was verified, for both the deposition strategies, and independent of the deposition parameters selected. For both walls, there was a consistent excess of material deposited along the direction of the deposition guide line. This meant that, the strategy seen in 12 (a) had a larger length than intended, and, the strategy shown in 12 (b) had a width that was larger than projected.

This issue could not be overcame, as the alteration of deposition parameters, including modifications to the deposition parcel distance, did not change the position of the first and last deposition parcels, which were the ones that marked the beginning and end of the parts. Nonetheless, the depositions were carried out until all parameters were optimized, and the final measurements and deviations noted (tables 3.5 and 3.6).

Table 5: Final parameters for both the deposition strategies of the straight walls.

	WFS [m/min]	WTS [m/min]	CZ [m/min]	LH [mm]	Parcel Distance [mm]
Wall-Horizontal Gide Line	4	6	5.5	2.25	5
Wall-Vertical Guide Line	4	7	6	2.25	4

Table 6: Straight wall's final measurements and respective deviations from the CAD.

	Wall-Horizontal Guide Line	Wall-Vertical Guide Line
Lenght [mm]	54.3	47.8
Lenght Deviation [mm]	4.3	-2.2
Width [mm]	9.9	14.5
Width Deviation [mm]	-0.1	4.5
Heigth [mm]	20.1	19.7
Height Deviation [mm]	0.1	-0.3

When making a direct comparison between both the strategies while generating the same part, it is then clear that, overall the deposition with the vertical deposition guide line was the most successful as it was also the closest to the desired dimensions.

4.5. Cross Shaped Intersection

Since this geometry was an intersection of two straight walls ,that were identical to the ones analysed in section 4.4, similar deposition parameters were used as a starting point, and then adjusted as necessary. Furthermore, the deposition strategy that, on that same section, was concluded to be more accurate, was also selected for this geometry for three reasons:

- As just mentioned, it was concluded previously that it produced the final geometry closest to the CAD's dimensions;
- A deposition path with a higher oscillation would result in smaller necking effects on the intersections of the segments [10];
- There was a software incompatibility when trying to apply the other strategy. This will be discussed further on this work.

As such, the final deposition used the following parameters: $WFS = 4m/min$; $WTS = 6m/min$; $CZ1 = 6 : 5m/min$; $CZ2 = 1.4m/min$; $LH = 2.25mm$; Segment Distance $= 4mm$.

Unsurprisingly, the dimensions of the cross shaped intersection followed the same tendency of the straight wall's, as seen in table 4.7, where V indicates that regards the vertical segment of the part (along the Y axis), and H the horizontal one (along the X axis). However, it's interesting to note that even though both the average width and height of both segments are identical, the length differed in about one millimetre.

Table 7: Cross shaped intersection final dimensions and respective deviations from the CAD.

	Length-V	Length-H	Width-V	Width-H	Height-V	Heigth-H
Part Dimension [mm]	54.6	55.6	10.4	10.4	20.5	20.5
CAD Deviation [mm]	4.6	5.6	0.4	0.4	0.5	0.5

In regards to the intersection area, it was built as intended, without any lack nor excess of material, that could caused that section to have a different height than the rest of the part. However, after examining the sections adjacent to the intersection area, it was possible to locate necking effects, caused by a lack of deposited material (figure 13). Although the appropriate response would be to decrease the area of the WTS custom zone used, the software did not allow to decrease it any further. This problem was caused as the program requires the segments that outline the custom zones, to intersect either the part or the deposition segment. This means that a custom zone that's completely enclosed, by the part or segment, will not be recognized by the system.

Figure 13: Necking effect found on areas adjacent to the intersection area.

As mentioned on the beginning of this section, some problems were encountered while testing deposition strategies. When trying to divide the part into two "L" shaped deposition segments, the software did not recognize the segments, and thus did not generate a deposition path. It was also attempted to combine the use of two rectangular deposition segments, combining both the deposition strategies tested in section 4.4, but once more, the software wasn't successful in generating the deposition paths, although it did recognize the segments. Both of the aforementioned strategies were attempted as a way to emulate the results obtained by [11] and [12], for optimized deposition crossing.

4.6. Staircase Vertical Increment

Advancing to the final geometry studied, another software related problem arose right from the start. It was found that, when planing depositions that required several deposition segments and velocity custom zones, despite no error message nor visible problem was presented in the program's interface, upon inspecting the resulting files, meant to be sent to the KUKA robot, it was found that they were correct only until a certain layer. From that layer onwards, all the remaining files would be blank, suggesting that the software possessed a maximum amount of deposition segments and custom zones, that was capable to process at once. It was then necessary to separate the deposition into several ones, as if it were different parts to deposit. With each deposition, different layer files were saved and then all of them were combined at the end to comprise the complete deposition.

The final part was obtained using the following deposition parameters: $WFS = 4m/min$; $WTS = 5.5m/min$; $CZ = 4m/min$; LH = 2.5mm; Deposition Parcel Distance= 4mm.

Table 8: Staircase vertical increment final dimensions and respective deviations from the CAD.

	Step 1	Step 2	Step 3	Step 4	Step 5	Step 6
Length [mm]	9.1	10.6	9.2	10.6	11.5	15.1
Length Deviation [mm]	-0.9	0.6	-0.8	0.6	1.5	5.1
Width [mm]	11.8	11.4	11.7	11.7	11.5	12.1
Width Deviation [mm]	1.8	1.4	1.7	1.7	1.5	2.1
Heigth [mm]	11.2	5.2	5.1	5	5	3.9
Heigth Deviation [mm]	1.2	0.2	0.1	0	0	-1.1

Analysing the results, its possible to detect some overall tendencies in the results. As the Z coordinate increases on the part,the length of each step decreases, and with it, the surface area that is available to exchange heat with the environment. This decrease in the heat exchanged, along with a constant heat input, will ultimately result in an increase of the part's internal temperature. In turn, a higher heat input will maintain the material molten and more fluid. This then causes the molten material to spread along the width and length of the part, thus increasing these same dimensions. It's then possible to corroborate this effect, as there is an overall increase in both the length and width of the part, as seen in table 3.8, where "Step 1" represents the step closest to the substrate, and so forth.

Additionally, as the molten material migrates to the edges of the part, and increases the aforementioned dimensions, the height of each step decreases. Once again, this effect becomes more evident, the higher the Z coordinate of the part.

4.7. Final Test Artifact

Once all geometries were optimized and analysed, the final step was to group them and create the test artifact itself, as see in figure 14.

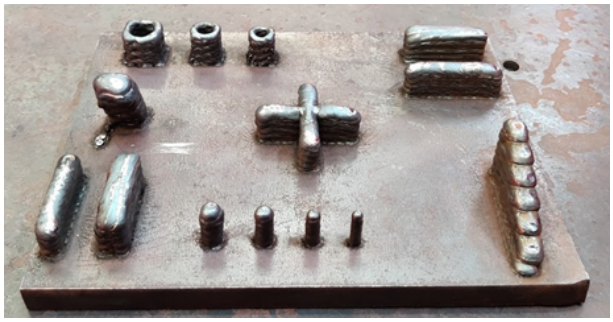

Figure 14: Final deposition of the projected test artifact.

Upon its manufacture, the user can then achieve similar informations, regarding the setup, as the ones presented throughout the previous sections. Furthermore, with the parallel placement of the straight walls, along the X and Y axes, it's also possible to evaluate the parallelism between them. As observed on table 3.9, it's possible to infer that the majority of the distance differences between them are minimal, likely caused by the bead surface waviness, and therefore negligible.

Table 9: Distances, in milimeters, between walls for both X-axis and Y-axis aligned walls.

X-Axis Straight Walls Distance [mm]	17.3	17.3	17.4	17.4	16.5
Y-Axis Straight Walls Distance [mm]	18.2	18.1	18.1	18.1	17.4

Both sets of walls also presented a significant distance difference at the end of the structures. This difference is likely associated with a material accumulation, generated at the beginning of each deposition. Lastly, it's possible to verify that while the average distance between the X-axis oriented walls was 17.98 mm, the one between the Y-axis oriented walls was 17.18 mm. This 0.8 mm difference could be correlated with an axis-specific deviation, but it's also important to mention that these two sets of walls were respectively the first and the last geometries being deposited on the final test artifact. Consequently, it's normal that there are some differences between them, in regards to the heat extraction capacities, and therefore, in their width values, thus affecting the distance between them.

4.8. Additional Setup Limitations

In addition to the setup induced limitations that were already described in the previous sections, the construction of the test artifact allowed to reveal some additional limitations.

Regarding the hardware, two distinct events were detected. The first occurred in an irregular and unpredictable way, throughout the depositions, but became clearer during the deposition of thin features, such as the thin pins. During the initial deposition phase, there was occasionally a slight delay with the electric arc ignition. As the robotic arm couldn't sense this delay, it began the designated trajectory, culminating in a slight bend and drag of the wire fed, until there was an ignition of the arc. Once the arc was ignited, the now distorted wire would then melt and promote material accumulation and shape distortions (figure 15 (a)).

The other effect arose consistently in all of the performed depositions. During the last section of every deposition, an unintended change in wire travel speed was detected. This velocity change was most noticeable when the robotic arm was asked to perform either under low or high speed, creating an easily observable difference in the amount of material deposited (figure 15 (b) and 15 (c)). This change in velocity was not intended by the end user, and as such, the code sent to the robotic arm didn't reference any changes to the velocity. This meant that there were no changes that could be made to the code in order to correct this, and was most likely a safety mechanism employed in the programming of the robotic arm.

(a) Material accumulation at the top of the thin pin, due to the arc ignition delay.

(b) Resulting deposited layer with a lower travel speed in the last deposition section.

(c) Straight wall aggravated dip, due to the increase of velocity at the end of each layer.

Figure 15: Outcomes of the hardware induced limitations.

5. Conclusions

The main objective that was set for this work, was to project and manufacture a test artifact that was specific to wire arc additive manufacturing (WAAM), while simultaneously providing the user with information regarding any geometrical limitation derived of the process's of the setup, either regarding software or hardware.

After the benchmark geometry selection, test artifact projection and manufacture, it was possible to extract the following information regarding the setup used:

- Partial overhangs were proven to be feasible, at least within the range of 60^o to 90^o with the substrate;
- The fabrication of thin features was compromised by software induced limitations, achieving nevertheless a diameter of 5.2 mm for the thin pins and 8 mm for the thin resolution holes;
- Both the straight walls, cross shaped intersection and the staircase vertical increment were compromised, by both hardware and software limitation. Despite this, the intersection was satisfactorily performed, with however the appearance of a necking effect in the adjacent areas. The vertical increments were affected by the increasing temperature of the part, but the measurements were satisfactory.

Ultimately, no significant deviations following the X, Y or Z axes were found, during the manufacture of the test artifact, hence suggesting that no recalibration, to the robotic arm's axes, was required. There were however problems with the timing of the electric arc ignition, as well as an undesired wire travel speed alteration, during the last deposition segments. These problems affected the final geometry of the parts and should be corrected.

Furthermore, as most of the setup imposed geometrical limitations were caused by the software used to generate the deposition paths, a more recent version of the WAAMSoft is advised.

References

[1] Baltej Singh Rupal, Rafiq Ahmad, and Ahmed Jawad Qureshi. Feature-based methodology for design of geometric benchmark test artifacts for additive manufacturing processes. *Procedia Cirp*, 70:84–89, 2018.

[2] Shawn Moylan, April Cooke, M Alkan Donmez, Kevin Jurrens, Shawn Moylan, and John Slotwinski. *A review of test artifacts for additive manufacturing*. US Department of Commerce, National Institute of Standards and Technology, 2012.

[3] Iso/astm 52902, 2019, " additive manufacturing—test artefacts—standard guideline for geometric capability assessment of additive manufacturing systems," astm international, west conshohocken, pa, standard no. iso/astm 52902:2019.

[4] Donghong Ding, Zengxi Pan, Dominic Cuiuri, and Huijun Li. A multi-bead overlapping model for robotic wire and arc additive manufacturing (waam). *Robotics and Computer-Integrated Manufacturing*, 31:101–110, 2015.

[5] Jun Xiong, Yangyang Lei, Hui Chen, and Guangjun Zhang. Fabrication of inclined thin-walled parts in multi-layer single-pass gmaw-based additive manufacturing with flat position deposition. *Journal of Materials Processing Technology*, 240:397–403, 2017.

[6] Donghong Ding, Zengxi Pan, Dominic Cuiuri, Huijun Li, Nathan Larkin, and Stephen Van Duin. Automatic multi-direction slicing algorithms for wire based additive manufacturing. *Robotics and Computer-Integrated Manufacturing*, 37:139–150, 2016.

[7] Nuno Pépe, Stephan Egerland, Paul A Colegrove, David Yapp, Andreas Leonhartsberger, and Americo Scotti. Measuring the process efficiency of controlled gas metal arc welding processes. *Science and Technology of Welding and Joining*, 16(5):412–417, 2011.

[8] Joining processes: Physiscs of welding arc. viewed on 2020-03-19.

[9] Xiangfang Xu, Jialuo Ding, Supriyo Ganguly, Chenglei Diao, and Stewart Williams. Preliminary investigation of building strategies of maraging steel bulk material using wire+ arc additive manufacture. *Journal of Materials Engineering and Performance*, 28(2):594–600, 2019.

[10] J Ding, F Martina, and S Williams. Production of large metallic components by additive manufacture–issues and achievements. In *Conf. Pap., nov*, 2015.

[11] Giuseppe Venturini, Filippo Montevecchi, Antonio Scippa, and Gianni Campatelli. Optimization of waam deposition patterns for t-crossing features. *Procedia CIRP*, 55:95–100, 2016.

[12] L Machado Santos Carvalho Neto. Studying the application of additive manufacturing to large parts. *Universidade de Lisboa, Lisbon*, 2017.